Universidad de La Laguna

Máster en Astrofísica

Especialidad Teórico Computacional

Trabajo Fin de Máster

SINGLE EPOCH ASTROMETRIC MICROLENSING

Raquel Forés Toribio

Tutor: Evencio Mediavilla Gradolph

Curso académico 2019/20

Index

Resumen

El efecto lente gravitatoria consiste en la desviación de rayos de luz de una fuente causada por un objeto masivo que se encuentra entre la fuente y el observador. De esta forma, pueden llegar más rayos de la fuente al observador produciéndose una especie de espejismo como los que se observan en la Tierra (Figura 1).

La ecuación que rige cómo se desvían los rayos de luz se conoce como ecuación de la lente (ecuación (6)). Las variables que intervienen en esta ecuación son variables angulares divididas entre el ángulo de Einstein (ecuación (5)) para adimensionalizarlas. Este parámetro es la escala característica de desviación de los rayos producida por una masa puntual M y también depende de las distancias entre la fuente, la lente y el observador. Para valores típicos de masas estelares y de distancias a galaxias para la lente y a quásares para la fuente, el ángulo de Einstein es del orden de microsegundos de arco. Por eso, el fenómeno de la deflexión de la luz procedente de un quásar por las estrellas de la galaxia lente se conoce como efecto microlente en quásares (*quasar microlensing*, en inglés).

La ecuación de la lente con la que se modela este efecto es la ecuación (14). Los parámetros característicos de un sistema lente son la convergencia o densidad superficial de masa adimensional (κ), la cizalladura o *shear* (γ) y la fracción de convergencia producida por las estrellas (α). La magnificación global de la imagen que produce el efecto lente se conoce como macro-magnificación y viene determinada por κ y γ, ecuación (12).

El efecto microlente distorsiona las imágenes de la fuente (un quásar en nuestro caso) induciendo desplazamientos de sus centroides. A partir de estos desplazamientos, se pueden estudiar tanto características de los elementos deflectores (la galaxia lente) como del objeto que está siendo magnificado (el quásar). A esta fenomenología y método de estudio se la denomina *microlensing* astrométrico y comienza a ser aplicable actualmente ya que los instrumentos pueden llegar a precisiones de unos pocos microsegundos de arco a la hora de determinar centros de distribuciones de luz.

En este trabajo proponemos fijar la referencia para medir el desplazamiento del centroide en una fuente lo suficientemente grande como para que el efecto de las microlentes no le afecte, como por ejemplo la región de líneas anchas (BLR, por sus siglas en inglés). El objeto de estudio del desplazamiento del centroide es el disco de acreción de los quásares que es mucho más pequeño y sí se ve afectado por las microlentes. Tanto el objeto de referencia como el objeto de estudio tienen características espectrales diferenciadoras, por lo que al observar con un espectrógrafo de campo integral (IFU, por sus siglas en inglés) se pueden separar sus imágenes y obtener el desplazamiento del centroide del objeto de interés con respecto al objeto de referencia con una sola observación. Es por esto que la técnica se puede denominar *microlensing* astrométrico en una única época.

El objetivo principal de este trabajo es proporcionar un estudio teórico sobre la aplicabilidad de este método. Para ello se comprobará la dependencia del desplazamiento del centroide con el tamaño de la fuente para tres sistemas lente distintos. Además, se estudiará la correlación entre los desplazamientos y la magnificación de la fuente.

Todo este análisis se lleva a cabo con un conjunto de rutinas que como resultado final devuelven el centroide de la imagen de una fuente (Figura 2). En primer lugar se computan posiciones aleatorias de las estrellas en el plano imagen de acuerdo con los parámetros del sistema lente. En caso de que sea necesario, se calcula el mapa de magnificación aplicando el método llamado trazado inverso de rayos (IRS, por sus siglas en inglés). Para que este mapa se corresponda con la magnificación sufrida por una fuente extensa, se debe convolucionar con la emisión de la fuente. De este mapa convolucionado se eligen posiciones donde centrar la fuente atendiendo a un rango de magnificaciones especificadas. Tanto si las posiciones son elegidas considerando la magnificación o no, se calcula la imagen de la fuente empleando el mismo método de IRS. Finalmente, se determina el centro de esta imagen haciendo uso de la ecuación (29). En cuanto a la referencia para el desplazamiento, se emplea el centroide de la imagen que se obtendría si toda la masa de la lente estuviera distribuida suavemente (ecuación (24)).

Los parámetros característicos de los sistemas lente estudiados se muestran en la Tabla 1. En primer lugar se ha estudiado visualmente la fenomenología del efecto microlente. En la Figura 4 se observa como las imágenes están alargadas en una dirección y comprimidas en la perpendicular a causa de la cizalladura externa. También se observa que el desplazamiento del centroide depende en gran medida de la posición de la imagen con respecto a las estrellas. Adicionalmente, se ha comprobado que el código desarrollado en este trabajo reproduce los resultados obtenidos por Treyer y Wambsganss (2004) (Figuras 5 y 6). El trabajo de estos autores consistía en estudiar el *microlensing* astrométrico fijando la referencia para el desplazamiento del centroide como la primera posición medida del objeto. Los principales inconvenientes del método que proponen son la necesidad de monitorizar los sistemas lente durante años y que los desplazamientos producidos por las microlentes se ven enmascarados por el movimiento relativo entre la fuente, la lente y el observador.

Como hemos comentado anteriormente el método bajo estudio de este trabajo, *microlensing* astrométrico en una única época, se basa en que el desplazamiento del centroide disminuya a medida que la fuente sea más grande. Sin embargo, en la Figura 8 se observa que no todos los sistemas lente cumplen esta tendencia. El sistema en el que no se observa una reducción del desplazamiento del centroide con el tamaño de la fuente se diferencia en que tiene mayor densidad de estrellas que el resto. Por lo tanto, no todos los sistemas lente serán apropiados para aplicar el método que proponemos.

Respecto a los resultados obtenidos en el estudio de la correlación entre el desplazamiento del centroide y la magnificación del flujo, se advierte que solo uno de los tres sistemas estudiados sigue una correlación positiva (Figura 10). Esto es debido a que los sistemas con macro-magnificación muy alta (en valor absoluto), deforman el espacio en mayor medida y, en consecuencia, la forma de las cáusticas (zonas donde

teóricamente la magnificación es infinita). En un sistema poco magnificado, las cáusticas se corresponden con posiciones donde hay estrellas cercanas y, por tanto, donde la desviación del centroide va a ser elevada. Sin embargo, si las cáusticas están muy elongadas, entonces se pierde la correlación entre zonas de alta magnificación y gran deformación de la imagen.

En lo referente a los valores que se esperan para los desplazamientos del centroide, se infiere que van a ser mayores cuanto mayores sean la macro-magnificación (en valor absoluto) y el ángulo de Einstein. No obstante, si los desplazamientos producidos por un sistema no son lo suficientemente elevados como para que puedan ser medidos, se pueden elegir eventos con magnificación alta. De esta forma, los desplazamientos esperados serán mayores, siempre y cuando el sistema presente una correlación positiva entre desplazamiento y magnificación. Otro factor a tener en cuenta, es que el objeto que se estudie debe tener un radio considerablemente menor que la distancia típica entre estrellas. De este modo, los desplazamientos que experimente serán mayores y más fácilmente medibles. Por el contrario, la fuente de referencia debe ser mayor que la distancia típica entre estrellas para que se vea afectada por el *microlensing* en la menor medida posible.

Aparte de estas conclusiones, se ha realizado un estudio sobre la consistencia de los resultados teniendo en cuenta las limitaciones prácticas de las simulaciones. En primer lugar, se ha examinado el efecto que tiene considerar un número limitado de estrellas en la determinación del centroide. Debido a que no se tiene una distribución infinita, siempre queda una fuerza residual que desplaza el centroide (Figura 11). Sin embargo, si se consideran suficientes configuraciones de estrellas, este efecto se promedia. Y en caso de que solo se considere una distribución de estrellas, la fuerza residual influye en todos los desplazamientos por igual por lo que las tendencias que se deduzcan seguirán siendo correctas. También se ha analizado el efecto que induce la resolución espacial que se elija en los cálculos. De este estudio se ha concluido que, si las fuentes se muestrean de tal forma que su radio ocupe cinco píxeles y se elija la misma resolución angular para el plano imagen, entonces los desplazamientos del centroide son lo suficientemente precisos.

Como trabajo futuro queda pendiente calcular los desplazamientos del centroide para modelos más realistas del disco de acreción para el objeto de estudio y de la BLR para la referencia. Además, es necesario optimizar el código empleado lo cual se puede lograr fácilmente paralelizándolo. Por otra parte, la estadística de los resultados mostrados también se debe mejorar incluyendo más sistemas lente y diferentes configuraciones de estrellas y fuentes. También proponemos estudiar la aplicabilidad de este método para restringir la abundancia de agujeros negros de masas intermedias ya que se comportan de manera análoga a las estrellas pero producen una desviación de los rayos de luz mucho mayor. Por lo tanto, se esperan desplazamientos mayores del centroide ya que estos son proporcionales al ángulo de Einstein y este depende de $\sqrt{M}$. Finalmente, si después de estas simulaciones se obtienen resultados positivos, se podría pasar a medir observacionalmente estas variaciones de los centroides empleando espectrógrafos de campo integral.

1 Introduction

1.1 Microlensing effect

1.1.1 Gravitational lensing

Since the light motion is defined by null geodesics, in a curved space-time the light will propagate following curved trajectories in general. Due to this reason, it is possible to detect more photons from an emitting source if a massive object is placed between the source and the observer because of the distortion of the space-time that causes the massive object. This effect is known as gravitational lensing and shown schematically in Figure 1 (a). The massive object in between is called the lens object. If the curvature of the light rays produced by this lens object is large enough, we can observe two (or more) images of the same source denoted by S_1 and S_2 in Figure 1. This phenomenon is analogous to the terrestrial atmospheric mirages.

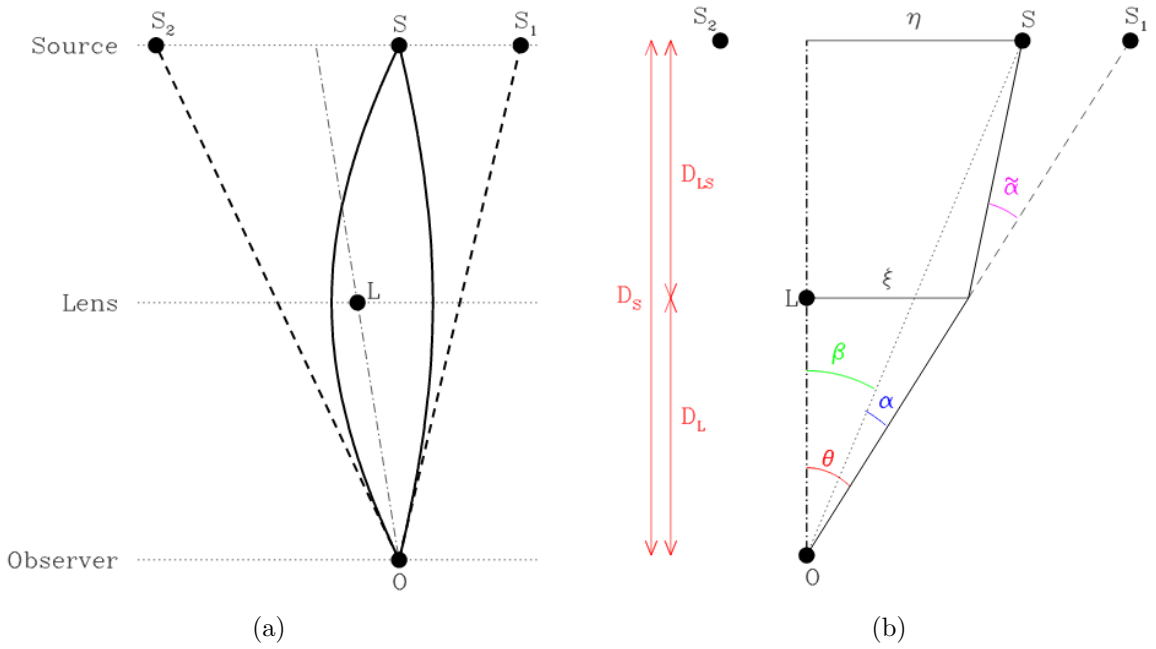

(a) (b)

Figure 1: Scheme of a gravitational lensing scenario where S is the source and $S_{1,2}$ are the images formed due to the deflection of light rays. In (a) the general path followed by the light rays is portrayed whereas in (b) the light path has been approximated to straight segments, the observer is aligned with the lens and only the ray that forms S_1 is pictured. Credit: Wambsganss (1998).

If the deflection is taking place at a small distance compared to D_L and D_{LS}, the light paths of Figure 1 (a) can be described by straight lines with an abrupt change of direction when they pass through the lens plane, namely, the thin lens approximation. The same figure in (b) shows this approximation with the observer aligned with the lens.

Note that in the figure above, for the sake of simplicity, it is considered only the plane formed between the line of sight and the light path. However, in order to map positions in the sky plane, it is necessary to consider two angles or two projected distances. Therefore, the angles and projected distances in the sky plane must be two dimensional vectors.

From General Relativity, the deflection angle of a light ray that passes at a distance $\vec{\xi}$ of a point mass M is (Schneider 2006):

$$\vec{\tilde{\alpha}}(\vec{\xi}) = \frac{4GM}{c^2}\frac{\vec{\xi}}{\left|\vec{\xi}\right|^2}. \tag{1}$$

To express the position of the source ($\vec{\eta}$) in terms of the deflection angle ($\vec{\tilde{\alpha}}$) and the position of its image ($\vec{\xi}$), is necessary to transform the latter two quantities into distances in the source plane. This can be done taking into account that $\vec{\tilde{\alpha}}$ is very small and the Thales's theorem, which is valid for a curved space-time, for $\vec{\xi}$:

$$\vec{d}(S_1 - S) = D_{LS}\vec{\tilde{\alpha}}\ ; \quad \vec{d}(S_1) = \frac{D_S}{D_L}\vec{\xi}.$$

Thus, the position of the source with respect to the origin in the sky plane is:

$$\vec{\eta} = \vec{d}(S) = \vec{d}(S_1) - \vec{d}(S_1 - S) = \frac{D_S}{D_L}\vec{\xi} - D_{LS}\vec{\tilde{\alpha}}(\vec{\xi}). \tag{2}$$

This equation is known as lens equation and can be expressed in other forms as shown below. For instance, it can be written exclusively in terms of angles by dividing it by D_S:

$$\vec{\beta} = \vec{\theta} - \vec{\alpha}(\vec{\theta}), \tag{3}$$

where it has been defined $\vec{\alpha}(\vec{\theta}) \equiv \frac{D_{LS}}{D_S}\ \vec{\tilde{\alpha}}(D_L\vec{\theta})$. Developing this expression by including the equation (1) for $\vec{\tilde{\alpha}}(D_L\vec{\theta})$, one can obtain:

$$\vec{\alpha}(\vec{\theta}) = \frac{D_{LS}}{D_S}\vec{\tilde{\alpha}}(D_L\vec{\theta}) = \frac{D_{LS}}{D_S}\frac{4GM}{c^2}\frac{\vec{\theta}}{D_L\left|\vec{\theta}\right|^2} = \theta_E^2\frac{\vec{\theta}}{\left|\vec{\theta}\right|^2}, \tag{4}$$

where the Einstein's angle, θ_E, has been defined as:

$$\theta_E \equiv \sqrt{\frac{4GM}{c^2}\frac{D_{LS}}{D_S D_L}}. \tag{5}$$

If the Einstein's angle for a given system configuration is of the order of microarcseconds, then the gravitational lensing effect is generally called microlensing effect. By introducing typical distances to a galaxy for the lens object and to a quasar for the source and masses of the order of stars, the Einstein's angle obtained is about this order of magnitude and the effect is called quasar microlensing. Hence, if the matter

in the lens object is granulated in form of stars or other compact objects, the light rays are affected by these objects and micro-images of the source are formed.

If equation (3) is divided by the Einstein's angle, the lens equation can be rewritten as:

$$\vec{y} = \vec{x} - \vec{a}(\vec{x}). \tag{6}$$

The following definitions have been made in this equation:

$$\vec{y} \equiv \frac{\vec{\beta}}{\theta_E} = \frac{D_S \vec{\beta}}{D_S \theta_E} = \frac{\vec{\eta}}{\eta_0}, \tag{7}$$

$$\vec{x} \equiv \frac{\vec{\theta}}{\theta_E} = \frac{D_L \vec{\theta}}{D_L \theta_E} = \frac{\vec{\xi}}{\xi_0}, \tag{8}$$

$$\vec{a}(\vec{x}) \equiv \frac{\vec{\alpha}(\theta_E \vec{x})}{\theta_E} = \frac{\vec{x}}{|\vec{x}|^2}. \tag{9}$$

where the parameters η_0 and ξ_0 are the Einstein's radius in the source and the lens plane, respectively.

1.1.2 Microlensing lens equation

In the previous section the general formula for the lens equation has been derived (equation (6)). However, it has been only considered the deflection angle produced by a point mass. This section is going to present other deflection angles corresponding to different mass distributions of the lens object.

Firstly, the deflection of rays produced by a uniform and smooth mass distribution is given by:

$$\vec{a} = \begin{pmatrix} \kappa + \gamma & 0 \\ 0 & \kappa - \gamma \end{pmatrix} \vec{x}. \tag{10}$$

The parameter γ is known as shear and accounts for the possible external anisotropy of the gravitational field. The other parameter, κ, is denominated convergence or dimensionless surface mass density and is defined as (Schneider et al. 1992):

$$\kappa \equiv \frac{\Sigma}{\Sigma_{cr}} \; ; \quad with \;\; \Sigma_{cr} = \frac{c^2 D_S}{4\pi G D_L D_{LS}}, \tag{11}$$

where Σ is the surface density of the lens system and Σ_{cr} is the critical density which distinguishes between strong lenses and weak lenses. Strong lenses (with $\kappa > 1$) are able to produce multiple images of the source whereas weak lenses are not.

The effect of the parameters κ and γ in the image that the lens produce can be studied by solving the equation (6) for $\vec{x}$. The role of κ is to enlarge the size of the image and this increase will be larger as κ becomes closer to 1. On the other hand, γ deforms the image by elongating it in one direction and compressing it in the perpendicular direction. Depending on the combined value of these parameters, the image can be inverted with

respect to one axis or both in relation to the original source. These effects are quantified by the parameter μ which is called the macro-magnification (Schneider et al. 1992):

$$\mu = \frac{1}{(1-\kappa)^2 - \gamma^2}. \tag{12}$$

If this parameter is less than 1 in absolute value, the image produced will be smaller than the source. On the contrary, if $|\mu| > 1$, then the image will be bigger than the original source. In addition, a negative macro-magnification implies that the image has been inverted with respect to one axis.

Other configuration for the lens object can be a point mass positioned at $\vec{x_0}$ with external shear. This type of lens is known as Chang-Refsdal lens (Chang & Refsdal 1984) and the deflection that it produces is:

$$\vec{a} = \begin{pmatrix} \gamma & 0 \\ 0 & -\gamma \end{pmatrix} \vec{x} + \frac{\vec{x} - \vec{x_0}}{|\vec{x} - \vec{x_0}|^2}. \tag{13}$$

The second term of this equation is very similar to the deflection angle in equation (5) but here the mass is situated in the position $\vec{x_0}$ with respect to the origin of coordinates.

A more complex lens configuration, based on the two previous ones, is a distribution of n point objects with different masses embedded in a smooth mass distribution with external shear. The deflection that this system causes is studied in Schneider el al. (1992) and its expression is:

$$\vec{a} = \begin{pmatrix} \kappa_s + \gamma & 0 \\ 0 & \kappa_s - \gamma \end{pmatrix} \vec{x} + \sum_{i=1}^{n} m_i \frac{\vec{x} - \vec{x}_{i,0}}{|\vec{x} - \vec{x}_{i,0}|^2}, \tag{14}$$

where κ_s is the convergence of the smooth mass distribution and m_i is the quotient between the mass of the i-th object and the mass considered in the Einstein's angle. Typically, the Einstein's angle is defined with the mean mass of the compact objects.

This equation can model the deflection of light produced by a galaxy where the compact objects are stars and the smooth mass distribution represents the dark matter content. The convergence caused by the mass in stars is denoted as κ_* and the total convergence is the sum of both convergences: $\kappa = \kappa_s + \kappa_*$. The fraction between the convergence in stars and the total convergence is defined as:

$$\alpha = \frac{\kappa_*}{\kappa}. \tag{15}$$

The convergence of the stars as a function of the number of stars in a certain area can be expressed as:

$$\kappa_* = \frac{\Sigma_*}{\Sigma_{cr}} = \frac{M n_s / A}{M/(\pi \xi_0^2)} = \frac{\pi n_s}{A_x}. \tag{16}$$

It has been taken into account that the surface mass density in stars is the mean mass of the stars multiplied by all the stars and divided by the area considered. The critical surface mass has been expressed in terms of the Einstein's radius in the lens plane, ξ_0. Lastly, the symbol A_x expresses the area in units of the Einstein's radius in the lens plane squared, i.e., in terms of the dimensionless quantity x squared.

1.2 Impact of microlensing on quasar astrometry

By studying the effect of the microlenses on lensed quasars, it is possible to infer properties concerning both the microlenses and the quasars: whether there are compact objects within the lens object and, if so, which is their the mass distribution, and the size and brightness profile of the quasars (Wambsganss 2006).

In order to draw conclusions about these properties, the classical approach is to measure changes in the brightness of the images (Mediavilla et al. 2009). The variability and the amplitude of these variations are related with the size of the quasar and with the density of compact objects in the lens. These changes in brightness are produced by the relative movement between the observer, the microlenses and the source. However, in order to achieve statistically significant results, these systems must be monitored during long periods of time, typically over years.

Future improvements in astrometric instrumentation may allow a new approach to study the microlensing effect. The main idea is to measure the centroid of the images and study their shifts, instead of their variability in brightness. Several methods have been proposed whose main differences are the references chosen to measure the displacement of the centroid. Some examples of different methodologies are explained below.

A possible baseline for the displacements can be a theoretical reference obtained for a computational model of the lens system. However, the errors in the model can be greater than the displacements expected for a lens system with stellar compact objects, i.e., with masses around $1M_{\odot}$ (Oguri et al. 2013).

Another procedure proposed by Treyer & Wambsganss (2004) consists in fixing the reference in the first measured position of the centroid. The main drawback of this approach is that relies on measures over months or years as the classical method to study microlensing based on changes in magnitude. In addition, the accumulated movement masks the displacements produced by microlensing.

The third approach, which is the one this work is devoted to, consists in choosing a larger component of the quasar as a baseline. The principal hypothesis is that the larger component will be less affected by the microlensing effect since the distortions produced by the stars will be diluted. The most important advance that provides this method is that it can be applied with single epoch measurements since their reference does not depend on previous measurements.

A main element of interest in a quasar is its accretion disk (Jiménez-Vicente et al. 2014). This disk is usually described by the thin accretion disk theory (Shakura & Sunyaev 1973) which predicts that the temperature profile is $T \propto r^{-3/4}$. Therefore, different regions of the quasar accretion disk will predominantly emit in different wavelengths (Muñoz et al. 2011). The average radius of the quasars' disks is in the range from 1 to 4 light-days depending on the observed wavelength.

The component taken as the reference can be the Broad Line Region (BLR) whose spectral signature is the presence of very broad emission lines as its name indicates. This region is constituted by matter at high velocities and have a radius up to 1000 light-days (Zu et al. 2011).

Given the fact that a quasar presents regions with different sizes and different spectral characteristics, it is possible to determine in a single measure the centroid displacements of the disk at various radii by selecting different ranges of the spectrum. For example, the accretion disk has a continuum emission from the X-rays to the infrared depending on the radius considered. On the other hand, typical emission lines from the BLR are C III], C IV or Mg II whose wavelengths are typically observed in the optical range. The spatial distribution of different features of the spectrum can be determined using an Integral Field Unit (IFU) which segments the field of view in small portions and produces an spectrum of each portion.

Now, we are going to discuss the viability of measuring the centroid displacements of the microlensed images with current and future telescopes. Initially, it is natural to think that the angular resolution of a telescope is restricted by the diffraction limit given by the Rayleigh criterion: $\sigma = 1.22\lambda/D$. However, this limit gives the minimum angular separation between two objects in order to differentiate them. While, we are interested in measuring the centroid of the image. The lower limit for the angular error in the determination of this centroid for a telescope with a circular aperture was given by Lindegren (1978):

$$\sigma = \frac{\lambda}{\pi D\sqrt{N}}, \tag{17}$$

where λ is the wavelength, D the diameter of the telescope and N is the number of photons. Hence, as more photons from the image are detected, more precise will be the centroid determination. With this equation, we can estimate the minimum expected error in the centroid determination for a given telescope. A first example can be the VLT where MUSE is installed. By putting numbers for this instrument (diameter of 8.2 m, wavelength of 700 nm and 10^5 photons), the error in the centroid will be at least 18 microarcseconds (μas). In the future, an IFU for the ELT is planned, called HARMONI, which will be operating in the near-infrared range. For the specifications of this instrument (D=39 m and λ=1.46 μm) and the same number of photons, the error will be around 8 μas. Since the order of magnitude of the light rays' deflection for a single star in quasar microlensing is about microarcseconds, it is now becoming possible to measure directly the centroid variability for this effect. The only restriction is that the distribution of light of the image must be sampled by at least two pixels, criterion given by the Nyquist sampling theorem.

2 Objectives

The principal aim of this work is to analyze the prospects for applying single epoch astrometry to study the impact of microlensing on lensed quasars. This study is performed by means of three simulated lens systems with diverse lens parameters (Einsteins's radius in the source plane, shear, convergence and fraction of mass in stars). The deflection produced by each microlens is modelled using the Chang-Refsdal lens equation and including a smooth mass distribution.

The basic idea is to measure centroid displacements caused by microlensing with a single epoch of observations. The reference for zero shift will be a region sufficiently large so that it will be insensitive to microlensing. Thus, the main requisite to apply the single epoch method is that the displacement produced by the stars will be decreasing as the source grows larger. In order to prove if this requirement is fulfilled, the dependence of the centroid displacement with the size of the sources for the three lens systems will be studied. In addition, this work will provide an estimate of the magnitude of the expected displacements for each lens system.

Besides, an analysis on the correlation between highly magnified events and the centroid displacements associated to them will be conducted. If a positive correlation is to be found, then the displacements that could be measured will be larger by selecting only high magnification events.

Apart from the study of the applicability of this method, the aforementioned analysis will shed light on the behaviour of the centroid displacements under different conditions (i.e., different source sizes and different magnification values) for complex lens systems depending on their characteristic parameters.

3 Methodology

3.1 The image(s) of a lensed source

When studying gravitational lensing, it is customary to place the plane where the image is formed at the same distance as the lens object. This is convenient because the deflection angle and the lens equation are always expressed in terms of distances in the lens plane, $\vec{\xi}$. That is why this plane is usually called image plane even if features of the lens object are being discussed.

In order to achieve an analytical expression of the image that a lens object forms of a given source, inverting the equation (6) is necessary, i.e., we need to know $\vec{x}(\vec{y})$. However, this inversion is not trivial in most cases and the inverted equation is usually multivalued. Due to this reason, the problem is solved numerically by following a method known as "Inverse Ray Shooting" (IRS) developed by Kaiser et al. (1986) and Schneider & Weiss (1987, 1988).

This method consist in sampling the image plane, so a set of $\vec{x}$ are considered. This values are inserted in the equation (6) obtaining a $\vec{y}$ in the source plane for each position of the image plane. This is possible because equation (6) is always single-valued. Then the intensity value in a position $\vec{x}$ in the image plane ($I(\vec{x})$) is set equal to the intensity of the corresponding $\vec{y}$ in the source plane ($S(\vec{y})$). This process is performed according to the following scheme:

$$\vec{x} \xrightarrow{eq\ (6)} \vec{y}(\vec{x}) \Longrightarrow I(\vec{x}) = S(\vec{y}). \tag{18}$$

By applying this method to the whole image plane, it is possible to recuperate all the image(s) of the source when its light rays have been deflected by the lens object.

3.2 Magnification map

A magnification map contains information of how much a point in the source plane is going to be magnified by the lens object. In practice, we measure the fraction of area in the image plane that corresponds to a given pixel in the source plane. The strategy to compute this map is based on IRS but, instead of assigning an intensity to the image plane, it counts the times a particular $\vec{y}$ (corresponding to a pixel at the source plane) is obtained by applying the lens equation to a set of values $\vec{x}$. In order to do so, all the points in the magnification map must be set to zero initially ($M(\vec{y}) = 0$). The schematic procedure is shown below:

$$\vec{x} \xrightarrow{eq\ (6)} \vec{y}(\vec{x}) \Longrightarrow M(\vec{y}) = n + 1, \tag{19}$$

where n is the previous number of rays that fell in the position of the pixel $\vec{y}$.

Once this computation is done, it is useful to express the values of the magnification map with respect to the mean of the whole map, i.e., to divide the values of the magnification map by the mean value. On the one hand, this normalization is important since the number of counts on each position will depend on how many rays from the image plane are shot. Besides, the normalized magnification map will separate between the magnification produced by the macro-magnification (given by the mean) and the one produced by the microlenses (values different from the mean).

This argumentation is true if the source is a point but the sources have spatial extent. In order to ascertain the magnification for these extended sources, it is necessary to convolve the normalized magnification map ($M_{norm}(\vec{y})$) with the source emission ($S(\vec{y})$). This will produce a map in which each position $\vec{y}$ contains the magnification this source is going to suffer if its centroid is placed at $\vec{y}$. The convolved map is expressed mathematically in the following equation:

$$M_{conv}(\vec{y}) = \frac{1}{\int_{-\infty}^{+\infty}\int_{-\infty}^{+\infty} S(\vec{y}')dy_1'dy_2'} \int_{-\infty}^{+\infty}\int_{-\infty}^{+\infty} M_{norm}(\vec{y}-\vec{y}')S(\vec{y}')dy_1'dy_2'. \tag{20}$$

Note that the convolved map is already normalized because it is defined with $M_{norm}(\vec{y})$ and divided by the total intensity of the source.

3.3 Centroid determination

Given an image of a source, its centroid is determined in a similar way as the center of mass but, instead of having mass values, there is intensity values in the plane. Therefore, the expression used to obtain an image's centroid is:

$$\vec{x}_{cent} = \frac{1}{\int_{-\infty}^{+\infty}\int_{-\infty}^{+\infty} I(\vec{x})dx_1dx_2} \int_{-\infty}^{+\infty}\int_{-\infty}^{+\infty} I(\vec{x})\vec{x}dx_1dx_2. \tag{21}$$

In general, knowing the image of the source is needed in order to calculate the centroid. However, for a lens whose mass is distributed smoothly, the lens equation is easily invertible and hence the centroid in the image plane can be expressed as a function of the centroid in the source plane. The relationship between $\vec{x}$ and $\vec{y}$ is given by equations (6) and (10) and explicitly shown below:

$$x_1 = \frac{y_1}{1-\kappa-\gamma}\ , \quad x_2 = \frac{y_2}{1-\kappa+\gamma}. \tag{22}$$

Introducing this into equation (21), following the scheme shown in (18) and taking into account that the centroid of the source is defined analogously to the image's centroid, namely:

$$\vec{y}_{cent} = \frac{1}{\int\limits_{-\infty}^{+\infty}\int\limits_{-\infty}^{+\infty} S(\vec{y})dy_1dy_2} \int\limits_{-\infty}^{+\infty}\int\limits_{-\infty}^{+\infty} S(\vec{y})\,\vec{y}\,dy_1dy_2; \tag{23}$$

it is derived that:

$$\vec{x}_{cent} = \frac{\int\limits_{-\infty}^{+\infty}\int\limits_{-\infty}^{+\infty} S(\vec{y}(\vec{x}))\frac{\vec{y}}{1-\kappa\mp\gamma}\frac{dy_1}{1-\kappa-\gamma}\frac{dy_2}{1-\kappa+\gamma}}{\int\limits_{-\infty}^{+\infty}\int\limits_{-\infty}^{+\infty} S(\vec{y}(\vec{x}))\frac{dy_1}{1-\kappa-\gamma}\frac{dy_2}{1-\kappa+\gamma}} = \frac{1}{1-\kappa\mp\gamma}\frac{\int\limits_{-\infty}^{+\infty}\int\limits_{-\infty}^{+\infty} S(\vec{y})\,\vec{y}\,dy_1dy_2}{\int\limits_{-\infty}^{+\infty}\int\limits_{-\infty}^{+\infty} S(\vec{y})dy_1dy_2} = \tag{24}$$
$$= \frac{\vec{y}_{cent}}{1-\kappa\mp\gamma},$$

which gives the same relationship as the equation (22) and does not depend on the final image of the source. The upper sign corresponds to the component 1 of the vector; while the lower one, to the second component. This will be useful when fixing a theoretical reference to determine the shift that a source has suffered from passing its rays of light by a distribution of compact lens objects.

3.4 Algorithm implementation

In order to be able to compute the image and magnifications maps, the source and the image planes must be finite and have a finite spatial resolution, so that the computational time does not greatly exceed. Ultimately, the problem is dealt with squared matrices with a given number of pixels. It is necessary to link the pixel numbers in the matrices to their corresponding physical positions in the maps. This is done for a source plane with physical dimensions ranging from $-y_l$ to y_l using the following expressions:

$$i_1 = \left[\frac{y_1 + y_l}{y_s} + 1\right] \;,\;\; i_2 = \left[\frac{y_2 + y_l}{y_s} + 1\right] \;;\;\; with \;\; y_s = \frac{2\,y_l}{n_y - 1}, \tag{25}$$

where i_1 and i_2 are the row and the column of an element of the matrix, y_1 and y_2 are the physical positions in the plane and y_s is the scale relation between the physical size and number of pixels per side, n_y. The symbol [ ] expresses the integer part of the number inside it.

The relation between pixels and physical positions in an image plane starting at $-x_l$ and ending at x_l is analogous to the previous equation but now the matrix has n_x pixels per side, and the pixels are named j_1 and j_2:

$$j_1 = \left[\frac{x_1 + x_l}{x_s} + 1\right] \;,\;\; j_2 = \left[\frac{x_2 + x_l}{x_s} + 1\right] \;;\;\; with \;\; x_s = \frac{2\,x_l}{n_x - 1}. \tag{26}$$

All the heavy computational work has been conducted with *Fortran 90* so the previous expressions are particular for this programming language. The most important difference to take into account is that the array indexing starts at 1 as opposed to other languages such as *C*.

Since the image plane should contain all the images of the source but its size must be finite, the minimum half size of the map is set through the following expression:

$$x_l = \frac{1.5\ y_l}{min\{|1-\kappa-\gamma|, |1-\kappa+\gamma|\}}, \tag{27}$$

where κ is the total convergence of the lens. The most magnified axis is selected by choosing the minimum value in the denominator. This convention is adopted since distances in the image plane are elongated up to $\Delta y/(min\{|1-\kappa+\gamma|, |1-\kappa-\gamma|\})$ if all the mass were smoothly distributed. Additionally, a factor 1.5 is included since deflection of light by the microlenses can be occasionally larger than the smooth distribution (Mediavilla et al. 2016).

Due to the discretization of the space, the integrals (20) and (21) must be changed into finite summations, as follows:

$$M_{conv}(i_1, i_2) = \frac{1}{\sum_{i'_1=1}^{n_y}\sum_{i'_2=1}^{n_y} S(i'_1, i'_2)} \sum_{i'_1=1}^{n_y}\sum_{i'_2=1}^{n_y} M_{norm}(i_1 - i'_1, i_2 - i'_2) S(i'_1, i'_2); \tag{28}$$

$$j_{n,cent} = \frac{1}{\sum_{j_1=1}^{n_x}\sum_{j_2=1}^{n_x} I(j_1, j_2)} \sum_{j_1=1}^{n_y}\sum_{j_2=1}^{n_y} I(j_1, j_2) j_n\ , \quad with\ n = 1, 2. \tag{29}$$

In order to obtain the spatial coordinates of the image centroid (i.e., $\vec{x}_{cent}$), the result of the latter expression must be transformed solving the equation (26) for x_1 and x_2.

3.5 Flow chart of the computation procedures

All the simulations conducted follow the same scheme portrayed in Figure 2. In the first place, the lens system's parameters (κ, γ and α) along with the half side of the source plane and the seed for random generation of numbers are introduced in the routine *stars.f90*. This code returns the size of the image plane, the total number of stars within this plane and a file (*stars.dat*) with the random positions of the stars, $x_{i,0}$. After this computation, two different branches can be followed depending on whether the user is interested in the correlation between centroid displacement and flux magnification or not.

The latter case corresponds to the left branch of the diagram. Initially, a magnification map is computed making use of *magmap.f90* which needs as inputs the pixels per side of the source plane and of the image plane as well as the previous information. This routine computes the magnification map applying the IRS method. Once this map is computed, it must be convolved with the source. This is achieved by means of *magmap_conv.f90* whose inputs are the magnification map and the size of the source. After this computation, *select_pos.f90* chooses a position of the convolved magnification map (*magmap_conv.dat*) which has a magnification between m_{min} and m_{max}. This position will be the center of the source, $\vec{y}_{cent}$.

Regardless of the choice of $\vec{y}_{cent}$, *source.f90* takes the centroid of the source, its radius and the pixels of the plane and produces a file with the sampled source (*source.dat*). This file is taken along with the information of the number of pixels in the image plane by the routine *image.f90* to produce the image of the source applying the IRS method. Finally, the code *centroid.f90* computes the centroid of the resultant image ($\vec{x}_{cent}$) and saves it for posterior analysis.

The routines exposed in this diagram along with the ones employed for data analysis and representation (chiefly written in *Python 3*) are originals and developed by ourselves.

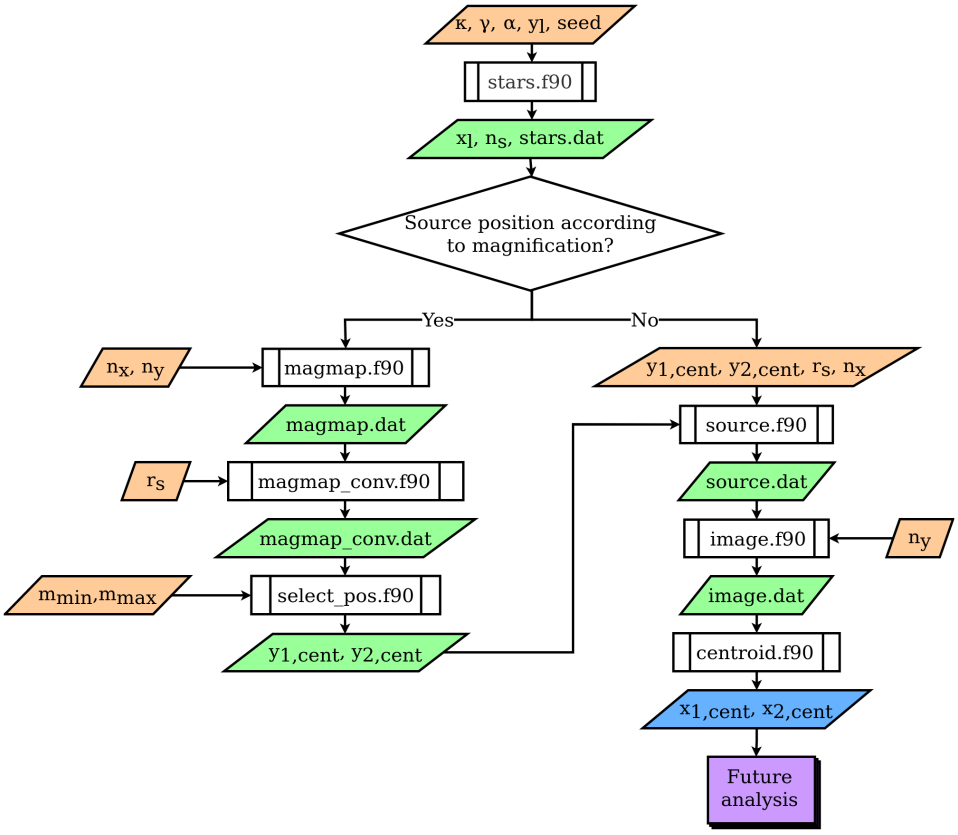

Figure 2: Flow diagram of the generic process applied during this work. Orange parallelograms are input information provided by the user, green parallelograms are intermediate results of the process and the blue cell is the final result. The routines employed are symbolised as a rectangle with vertical lines at its sides.

4 Results

4.1 Lens systems considered

Three different lens systems have been employed in order to study the behaviour of the centroid shift of images in different conditions. The lens systems considered are based on actual lens systems entirely with the exception of one system which is a combination of two lens systems. The specifications of each system, the actual systems which they are based on, and the name given in this work are displayed in Table 1.

Name	z_s	η_0 (ld)	γ	κ	α	μ	Based on
System A	1.69	38.22	0.40	0.36	1.0	4.01	Image A of QSO 2237+0305
System B	1.38	6.91	1.19	0.55	0.1	-0.82	Image B of SBS 0909+532
System C	1.69	38.22	0.59	0.44	0.1	-28.99	Image A of QSO 2237+0305 for z_s and η_0 Image A of RX J1131-1231 for the rest

Table 1: Name of the systems studied, redshift of the source (z_s), Einstein's radius of the source in light-days (η_0), shear (γ), convergence (κ), fraction of the convergence in stars (α), macro-magnification (μ) and the real systems which they are based on.

The redshift and the Einstein's radius are extracted from Mosquera & Kochanek (2011) where they assume to calculate the Einstein's radius a mean mass of $0.3M_{\odot}$. The shear and convergence are given by Mediavilla et al. (2009) and the macro-magnification is calculated using equation (12). The scale between a distance in the source plane and the angle that it subtends is calculated for a flat universe with Ω_M=0.286 and H_0=69.6 km/s/Mpc (Wright 2006). For an object with z=1.69, 1 ld subtends 0.097 μas and, for an object with z=1.38, 1 ld=0.098 μas. Owing to the dispersion of the values of Ω_M and H_0, the angular scale has been approximated for both systems to 1 ld=0.1 μas.

The fraction of convergence in stars is estimated taking into account the configuration of the system. The spatial configuration can be consulted in the CASTLES Survey and in Figure 3 are shown the lens systems that we use. The images of QSO 2237+0305 are seen through the bulge of the lens galaxy, so virtually all the mass is in stars. However, for SBS 0909+532 and RX J1131-1231 the images are seen through the halos of their lens galaxies where the proportion of stars is around 0.1.

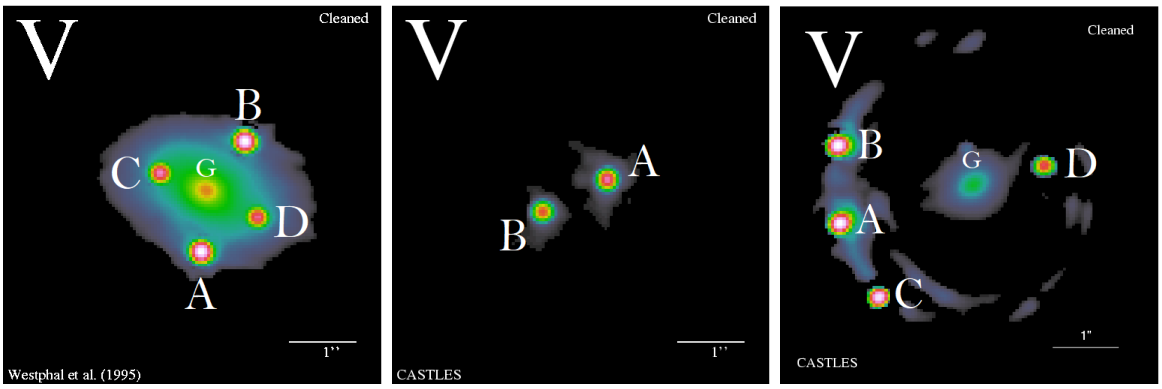

(a) (b) (c)

Figure 3: Images in visible light (filter F814W) of the lens systems: QSO 2237+0305 (a), SBS 0909+532 (b) and RX J1131-1231 (c). G is the lens galaxy and A, B, C and D are the multiple images that the system forms. Adapted from: CASTLES Survey.

4.2 Phenomenology

The aim of this section is to explain visually what procedure is applied and the initial expectations of the impact of the microlensing effect on the centroid of the lensed images. In the first place, a random distribution of stars with the same mass is placed in the image plane. The number of stars per area is fixed by κ_* and the size of the image plane must be at least equal to the criterion given by equation (27). The centroid of the images produced by a lens system is computed with equation (29). And the shift of the centroid is given with respect to the centroid of the image if all the mass were distributed smoothly, i.e., the modulus of the difference between the computed centroid and the centroid given by equation (24) where $\vec{y}_{cent}$ is the centroid position of the source.

Figure 4 shows the images of a source with a Gaussian emission profile with σ=4 ld and truncated at 12 ld from the center. This source is placed at three different positions in the source plane of system A. The centroid of its images and its shifts are also displayed in the plots. As it can be seen, different positions of the source yields to different images and shifts. Another interesting feature of these images is the elongation along the horizontal axis. This is specially noticeable for the far-right image of Figure 4 (c). The reason behind this deformation is the effect of the shear which elongates the space along the horizontal axis and compresses it in the vertical direction.

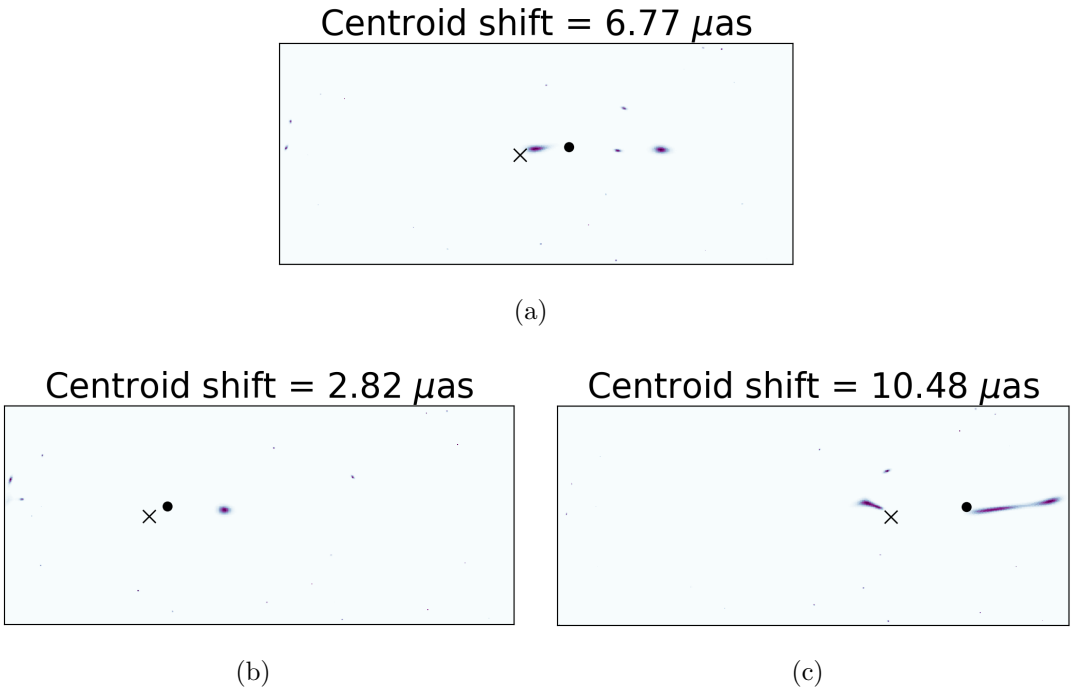

Figure 4: Images of a Gaussian source produced by lens system A for three different positions. The dot marks the position of the centroid of the images, the cross indicates the centroid if all the mass were distributed smoothly, and the distance between these points is shown at the top of the figures in microarcseconds.

4.3 Comparison with previous work

Treyer & Wambganss (2004) simulated the centroid shift of the images for a lens system with κ=0.6 and γ=0.6 with respect to an initial position of the centroid. A first step in the present work is to check whether our computations reproduce consistently their results. In order to do so, a source with radius σ=0.10η_0 and Gaussian emission profile is placed at consecutive positions along the elongated axis for lens system A, which is the lens system with more similar parameters to the ones considered by Treyer & Wambganss (2004).

By comparing Figure 5 with Figure 6 (a), it can be observed that the order of magnitude and the behaviour are quite similar although not identical. The differences arise from the different parameters taken for the convergence and shear. Another minor causes for the different displacements are the different source radius and the distribution of stars.

In Figure 6 (b) the approach proposed in this work is presented. The trajectory followed by the source is the same as the one in (a) but here the displacement is calculated with respect to the centroid of the image obtained if all the mass were smoothly distributed (i.e., in absence of microlensing). The most distinctive feature is that the displacement in the direction of the trajectory is not overshadowed by the

accumulated movement with respect to the origin in contrast to the previous approach. In consequence, the shift produced by microlensing is more evident. In addition, since the displacement does not depend on an arbitrary position in the past (given that we have a zero shift reference provided by a larger source), this method does not require a long-term tracking of the lens system.

A common behaviour in the three figures is that the modulus of the shift is dominated by the displacement in the elongated direction. The reason is that the shear will increase the small deviations in the elongated direction while it will compress them in the perpendicular direction. This is even more critical for the displacements with respect to an initial position because it also increases the displacement in the elongated axis as the source moves.

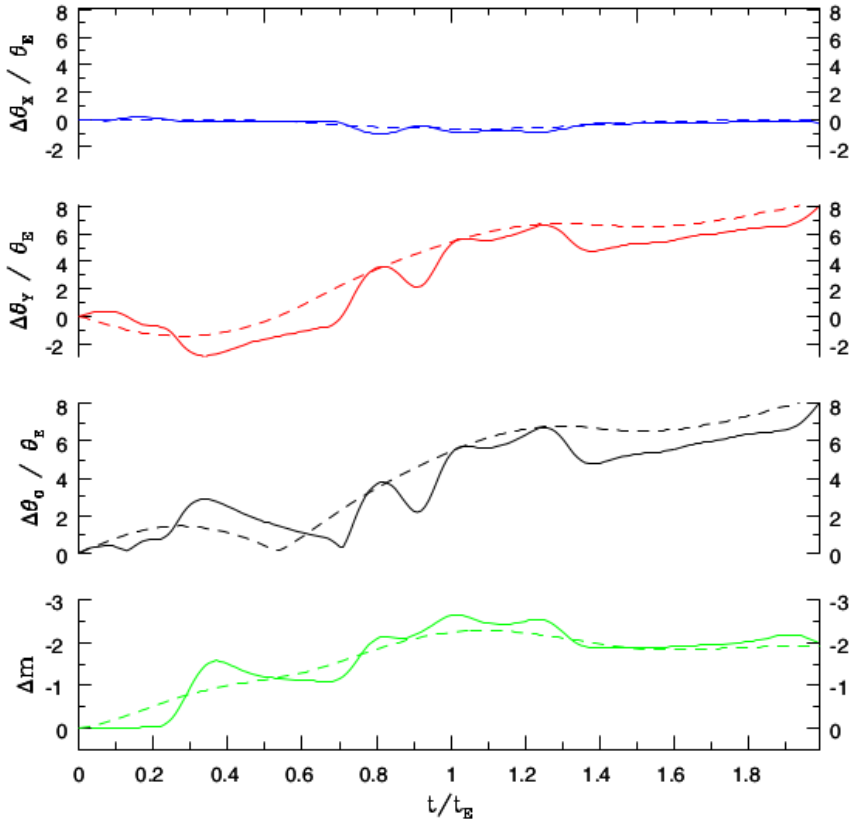

Figure 5: Displacements of the centroid in a lens system with κ=0.6 and γ=0.6 as the source moves in the elongated direction. The figures from top to bottom are: displacement in the compressed direction, displacement in the elongated direction, modulus of the displacement and changes in apparent magnitude. All the shifts are given in units of Einstein's angle and with respect to the initial position. Two sources are considered with radius σ=0.04η_0 (solid lines) and σ=0.16η_0 (dashed lines). Credit: Treyer & Wambsganss (2004).

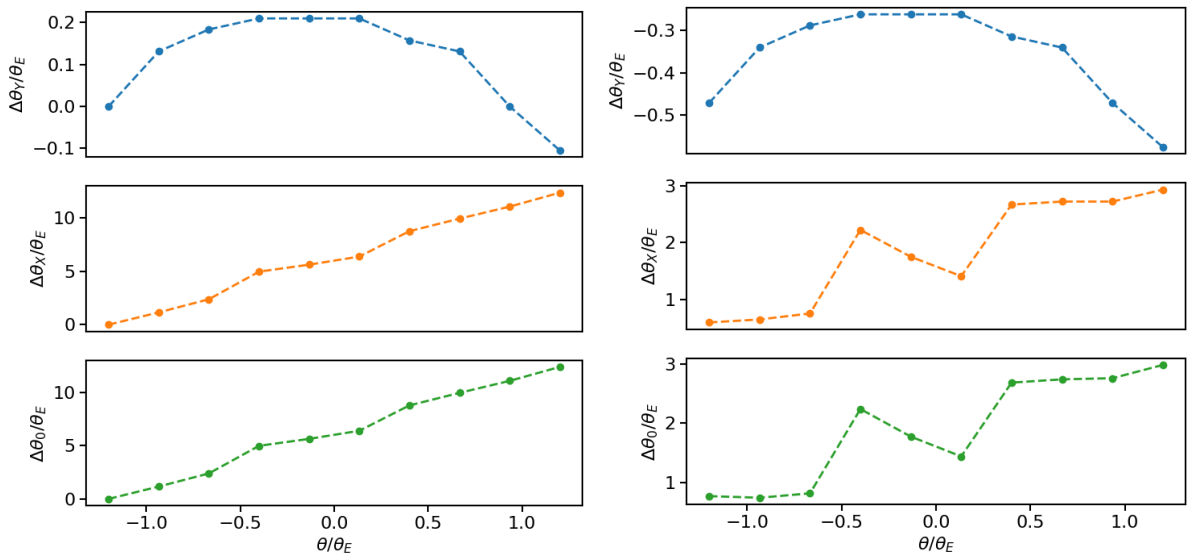

(a) (b)

Figure 6: Displacements of the centroid in system A as the source moves along the elongated direction, from top to bottom: displacement in the compressed direction, displacement in the elongated direction and modulus of the displacement; all in units of Einstein's angle. In (a), displacements of the source with respect to its initial position for a recreation of the simulation carried out by Treyer & Wambsganss (2004) with a source of σ=0.10η_0 during a similar trajectory length. In (b), displacements obtained for the same source and trajectory as in (a) but with respect to the centroid of the image in a smooth mass distribution.

4.4 Source size dependence

In the limit case of just one microlens, the dependence of the centroid shift with the size of the source is expected to follow a decreasing tendency. The justification is found in equation (13) because the deflection induced by the compact mass decreases with the distance to it. At large distances the equation becomes more similar to the equation (10) which is used for the reference of the centroid shift. As a result; if the source is larger, more regions of the image will be further away from the action of the star's distortion. If the star is placed at the center of the plane, the distortion will be symmetric, so that the centroid will remain in the center. This happens equally for the centroid of the smooth distribution system and, hence, the difference between them will be always null.

This is the reason why in Figure 7 the star was placed at $0.5\xi_0$ to the right of the center. Nine sources with constant emission profile and radii ranging from 5 to 200 ld where placed in the lens system A. However, as just one star is located, the convergence of this system is not preserved. As this figure shows, there is a clear decreasing tendency of the centroid shift as the source becomes larger. Despite that, it is necessary to analyze whether this tendency still remains valid for more complex systems (with more stars within the image plane) with different characteristic parameters.

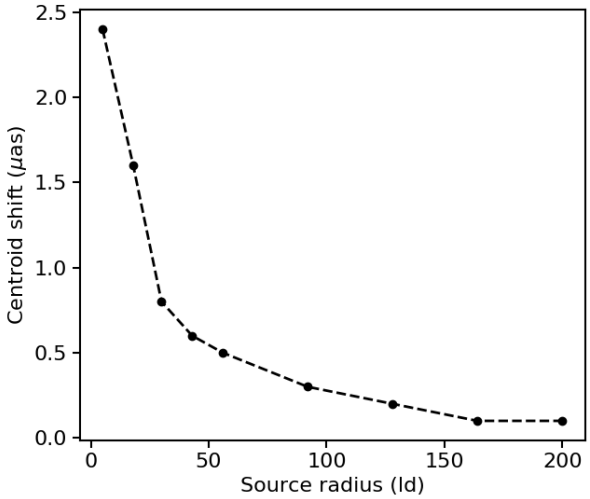

Figure 7: Centroid displacements in microarcseconds as a function of the source radius for system A. However, just one star is placed at $0.5\xi_0$ from the center so κ is not maintained.

Figure 8 is devoted to show the tendency for the three systems under study. For each system, 9 different size sources with constant emission are considered and their shifts were calculated for 20 random distribution of stars. The error bars are estimated as the standard deviation of the mean for 20 shifts for each source. The range of radii is selected in a way that the fifth source has the same size as the mean separation between stars, which marks a characteristic size for the sources ($\langle r \rangle$). The upper and lower limits of the radii are restricted by computer limitations. Too small sources require a higher resolution and too large sources require a source and image plane larger. Both limits imply that the number of pixels must increase and, in turn, more rays must be shot. In addition, more stars must be considered if the image plane is larger so on each computation of the inverse ray there will be more terms on the summation of equation (14). These effects contribute to increase the computation time.

The mean separation between stars is calculated as the square root of the mean area for a star, making use of equation (16):

$$\langle d \rangle = \sqrt{A_x/n_s} = \sqrt{\pi/\kappa_*}, \tag{30}$$

and the radius of the characteristic source for each system is the half of this expression:

$$\begin{aligned} \langle r \rangle_A &= 1.46\eta_0 = 56\ ld, \\ \langle r \rangle_B &= 3.78\eta_0 = 26\ ld, \\ \langle r \rangle_C &= 4.22\eta_0 = 161\ ld. \end{aligned}$$

As it can be seen, the source must be larger in terms of Einstein's radius as less mass is found in stars (lower κ_*). Nevertheless, this relation does not hold for the size in light-days because the Einstein's radii of the three systems are different.

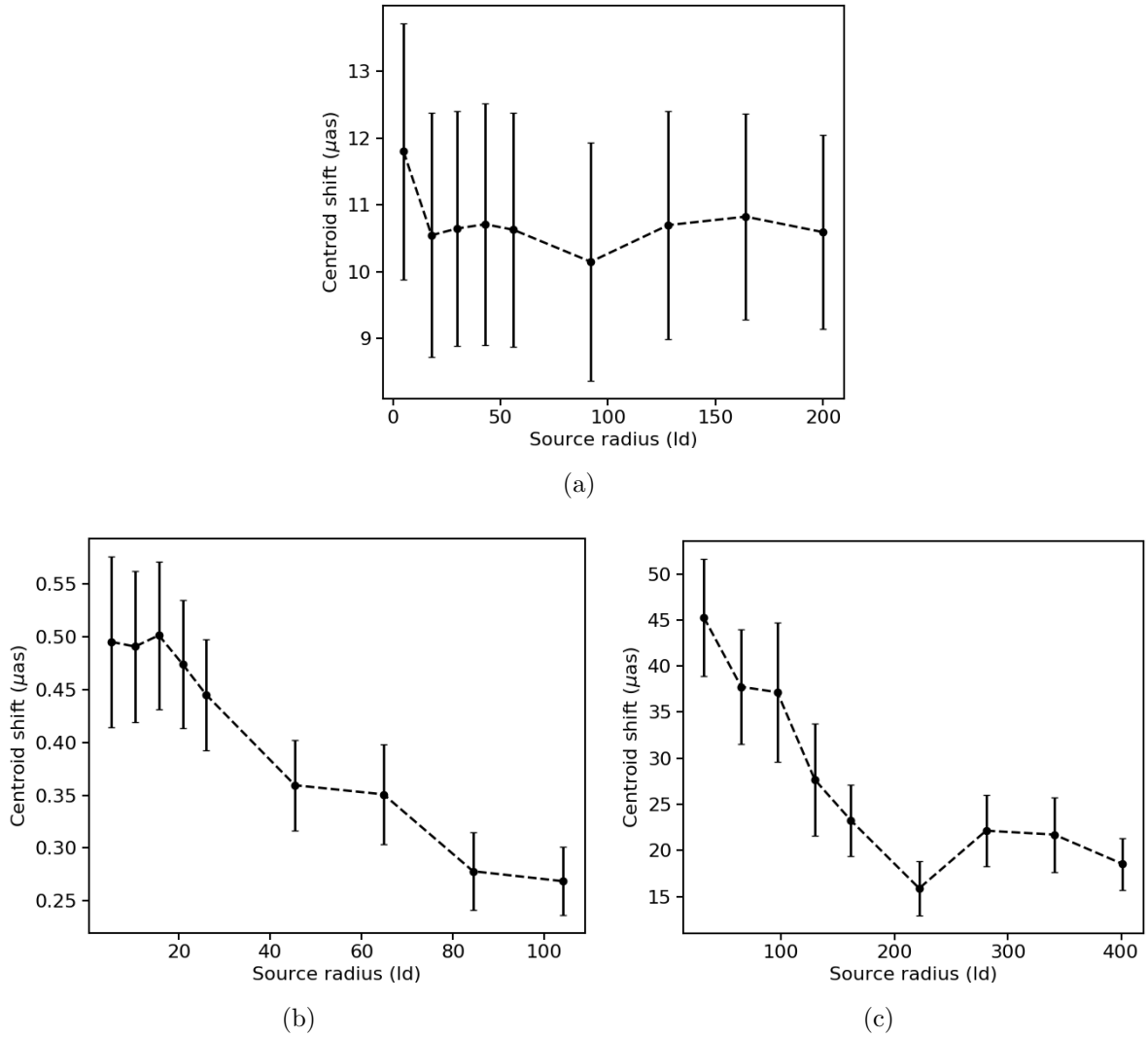

Figure 8: Shift of the centroid with respect to the radius of the source. There have been considered 20 random stars' distributions in order to calculate the error bars. The dependence for the lens system A is pictured in (a), for system B in (b) and for system C in (c).

From Figure 8 can be inferred that lens system A is the only system that does not preserve the tendency expected, its shifts remain virtually constant regardless of the source size considered. The main difference between this system and the rest is that the mass in stars is much larger: $\kappa_* = 0.36$ in contrast to 0.055 and 0.044, respectively.

Another interesting result of this study is that the centroid shifts are larger as the macro-magnification is greater in absolute value and as the Einstein's angle is larger. The explanation to this correlation is that the small deviations produced by the individual stars are amplified by the macro-magnification. In addition to this amplification, when these distortions are converted into physical angles, the values will be greater if the Einstein's angle of the system subtends a larger angle in the sky. This is why lens system B exhibits such small centroid shifts, it has the smallest value of macro-magnification

and Einstein's angle (where the Einstein's angle has been calculated dividing η_0 by the angular distance given by the redshift of the source). By comparing the centroid shifts scales of lens system A and C, it is clear that the macro-magnification parameter is relevant because, even having the same Einstein's angle, their shifts differ a factor 3.

4.5 Magnification dependence

The classical observational effect of microlensing is the magnification of the source. In this section we are going to ascertain to what extent microlensing magnification is correlated with the displacement of the centroid. With this aim, the dependence of the centroid shift with the position of a source of 1 light-day and constant emission is studied. This size for the source is chosen because it has the typical size of a quasar inner accretion disk.

In Figure 9 (a) the convolved magnification map for the lens system A is shown. The magnification map is obtained as explained in section 3.2 and the convolution with the source is computed using equation (28). The peculiar geometrical forms obtained are called caustics and they constitute a set of positions where the magnification is very high. This features appear in the vicinity of compact lenses. Theoretically, the caustics are lines without thickness where magnification is infinite. However, due to the finite resolution and the convolution with a extended source, the caustics are thicker and have finite values.

After the computation of the convolved magnification map, a histogram of its values is extracted in order to ascertain which range of the magnification values is going to be used. Since having positions with the exact same value of the magnification is too infrequent, then the histogram is computed for a bin width of 0.2. In this section, five center values of magnification are chosen. The criterion applied in order to decide the maximum value of the magnification is that the bin of the maximum magnification will have at least 50 counts. Then, for each magnification value, 50 positions are selected randomly in order to center there the source. This process must be done for each system since they have different distribution of magnifications values.

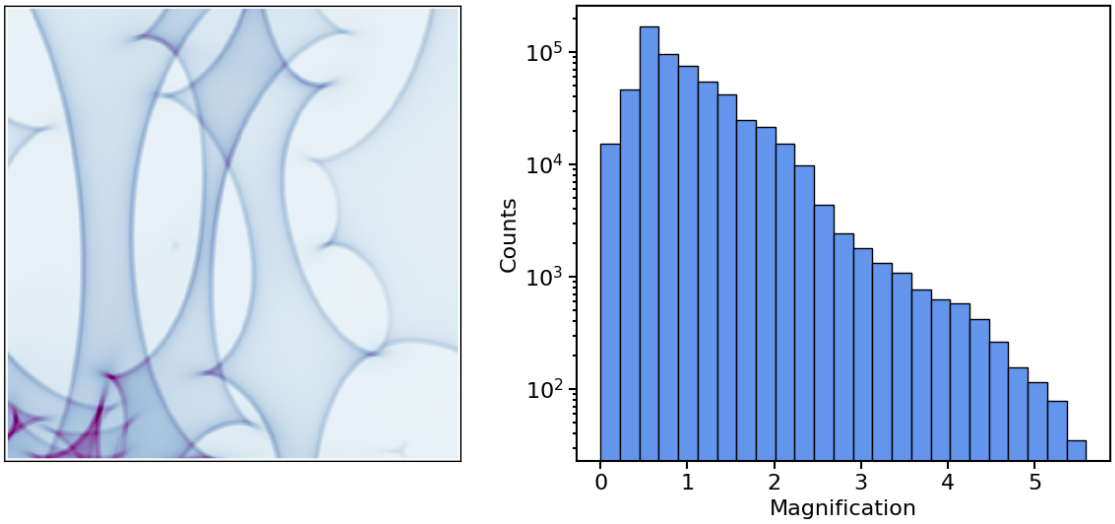

(a) (b)

Figure 9: Magnification map of the lens system A convolved with a source with radius of 1 ld and constant emission profile in (a). The histogram of the magnification values in logarithmic scale is portrayed in (b).

Once the positions of the source are determined, the images produced for the systems are computed and then their centroid shifts are obtained. For each magnification value, the mean of their shifts is calculated and the errors are estimated as the standard deviation of the mean. The results of this procedure are presented in Figure 10 where a weighted least squared fit is also performed.

The initial supposition is that, if the magnification is larger (i.e., more light rays from the source appear in the image plane), the centroid shift could be greater. However, this expectation is only true for system B which has a fit with positive slope (Figure 10 (b)). The underlying reason is the macro-magnification; if this parameter is large in absolute value, this means that the space is very magnified. In consequence, the caustics will be very distorted and the image does not have to be near a star in this case. Since the deflection of the stars is the responsible for the displacements of the centroid, then the centroid shifts in regions with high magnification do not have to be larger than the rest under high macro-magnification conditions.

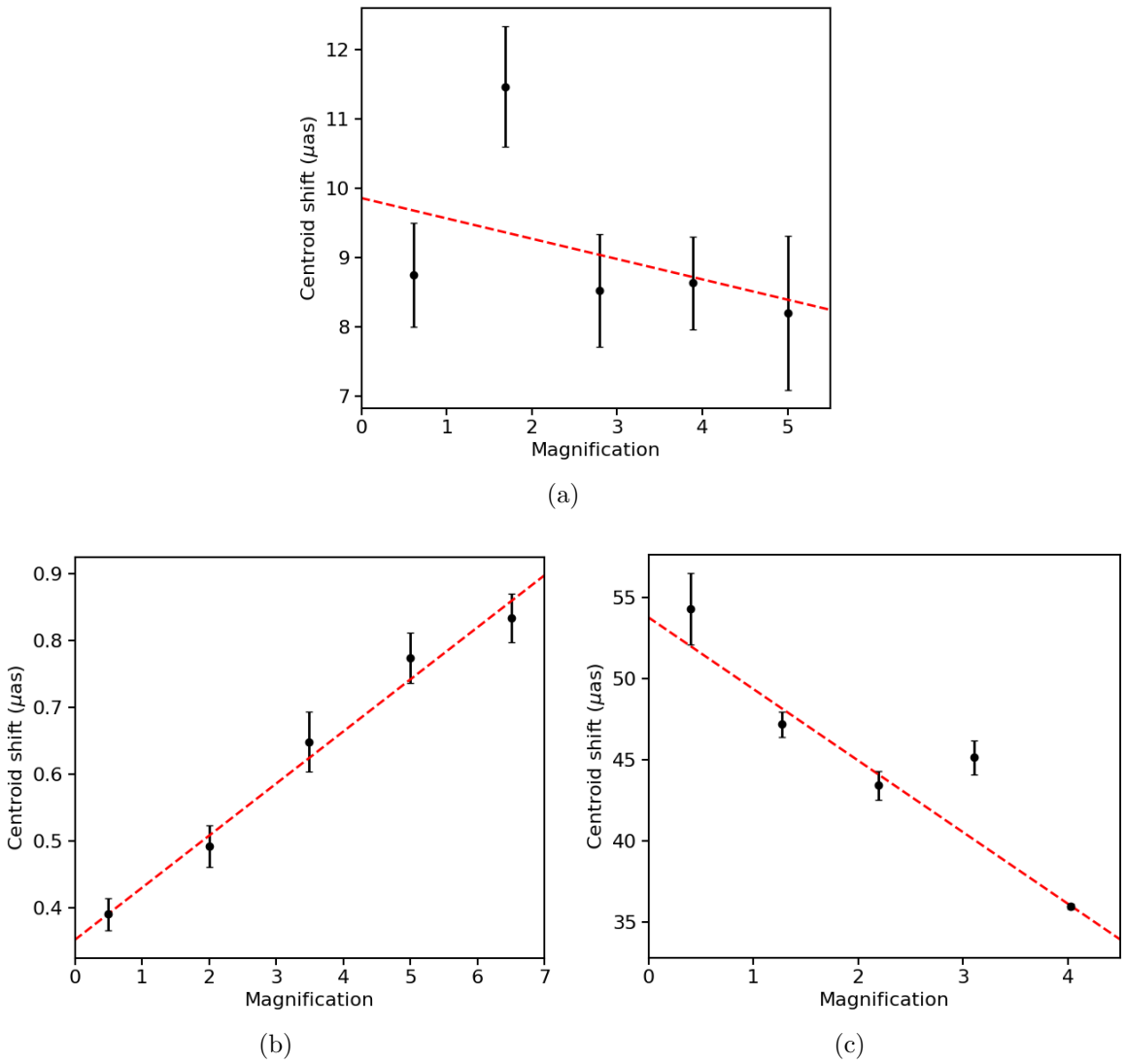

Figure 10: Dependence of the centroid shift with the magnification where a source of 1 ld is placed. Each point is the mean of 50 displacements and its error is the standard deviation of the mean. The dashed red line shows a least squared fit weighted with the inverse of the errors. Lens system A is shown in (a), system B in (b) and system C in (c).

There is a peculiarity in Figure 10 (c), the last point has an error too small compared with the rest of the points. The explanation for such a small standard deviation is because all points selected belong to the same region so the centroid displacements are rather similar. Given the extreme magnification of this system, only a portion of one caustic appears in the magnification map so not enough variability in positions is achieved.

Finally, in this figure can be seen the same effect stated in section 4.4, the centroid shifts will be greater when the Einstein's angle and the absolute value of the macro-magnification are larger. So this result becomes more robust since two independent approaches provide the same correlation of the centroid shifts with the macro-magnification and the Einstein's angle.

5 Discussion

5.1 Applicability of the method

In the light of the results exposed in the previous section, the single epoch method for astrometric measurements is going to be discussed. The first requirement to apply this method is a decreasing tendency of the centroid shift as the source size becomes larger. This is necessary since we need a zero shift reference. Thus, the reference must be a component of the quasar large enough so its centroid remains essentially unaltered by the stars' distortion. This region can be the Broad Line Region (BLR) of the quasar, whose radius can be up to 1000 ld in contrast to the 1 ld radius of the inner disk, which is usually the object under study. The systems that follow this desired tendency are the lens systems B and C (Figure 8). The main difference between these systems and system A is the mass contained in compact objects, so the systems suitable for applying this method should be systems with low κ_*. Fortunately, in the vast majority of known lens systems the fraction of mass in stars is small (Mediavilla et al. 2009).

However, this is not the only necessary condition for applying this method since there is an instrumental limitation for the angular resolution. Nowadays, the best angular resolution that can be achieved is around a few tens of μas, so not all the centroid shifts can be measured. Due to this reason, it is important to choose systems with a large absolute value of the macro-magnification and larger Einstein's angle, considering that in Figures 8 and 10 the larger shifts are obtained for systems with these specifications. Even when a lens system has relatively small centroid shifts, if it has little macro-magnification, then exists a positive correlation between high magnification events and large centroid displacements. Hence, by observing the system when a high magnification event occurs, measurable displacements of the image centroid can be obtained. Although this correlation holds for the lens system B, the centroid displacements are smaller than the current angular resolution even if high magnification positions are chosen at the magnification map. Nonetheless, this can be a plausible procedure for systems that have shifts just below the resolution limit.

Finally, it is also important the relationship between the radius of the characteristic source ($\langle r \rangle$), the radius of the object under study (r_s) and the radius of the object for reference (r_r). In order to obtain displacements of the object source large enough, its radius must be smaller than $\langle r \rangle$. And for the reference source, it is preferable to have the smaller displacement as possible so its radius must be greater than $\langle r \rangle$. If these conditions are fulfilled, then the measured displacement will be maximum and will have a minimum error.

In summary, the most suitable systems for applying this method will be the ones with a small fraction of mass in stars (κ_*), high absolute value of macro-magnification ($|\mu|$) and large Einstein's angle (θ_E). In addition to this requirements, the radius of the object under study and the radius of the reference must satisfy: $r_s < \langle r \rangle < r_r$ in order to achieve the maximum centroid difference and with the minimum error. However, these prescriptions do not give a precise set of parameters for which this method will yield measurable displacements. So, before observing a lens system, it is necessary to model the impact of astrometric microlensing in order to obtain an estimate of the expected centroid displacements.

5.2 Future work

The next natural step to take is to study the centroid displacements for more realistic sources in the lens systems that follow the adequate dependence with the source size, i.e., lens system B and C. The object sources will have a radius ranging from 1 to 4 light-days emulating the quasar accretion disk and the reference's radius will be 1000 ld as the BLR. By comparing the displacements of the sources with respect to the theoretical reference with the ones obtained with respect to the BLR, it will be possible to conclude whether this reference is able to reproduce properly the theoretical values of the displacements.

Regarding the employed code, a necessary improvement must be the reduction of the computation time. The simulation spends most of the time in the routines *image.f90* and *magmap.f90* where an Inverse Ray Shooting considering all the microlenses is being applied. The former routine can take around 20 minutes in order to obtain the image for one source in one position. In consequence, to obtain a point in Figure 10 (where 50 different positions of the source are being considered) can take around 16 hours of computation. An approach to reduce this computation time is to parallelize the code using the library *Open MPI*, as an example. This code can be parallelized without difficulty because the rays traced for each pixel are independent one from another, so the image matrix can be divided and sent to different processors.

Apart from the improvements that can be made in the code, it is equally important to increase the statistics of the results presented in this work in terms of more lens systems and more configurations. These different configurations are referred to different stars positions, a broader range in source sizes and more positions of the source depending on the magnification. Including more lens systems will help us to understand better the dependence of the centroid displacement with respect to the lens systems' parameters. Additionally, more statistic in different configurations will provide a more robust conclusions about this behaviour. This increase in the statistics is specially required for the centroid dependence with the magnification, since in section 4.5 only one distribution of stars were considered for each system.

This method can be also applied for different purposes apart from the research on sizes and temperature profiles of the accretion disks of quasars. Since the Einstein's angle depends on the square root of the mean mass of the compact objects (equation (5)), this procedure and its results can be extrapolated for different compact objects by multiplying the results for $\sqrt{M/(0.3M_{\odot})}$ where M is the mean mass of the compact objects and $0.3M_{\odot}$ is the typical stellar mass adopted in this work. For example, if the deflection of light is produced by intermediate mass black holes ($M \sim 500M_{\odot}$), the centroid shifts must be increased a factor 40. Hence, the expected displacements can be easily measured and they will enable the possibility of constraining the abundance of these objects in galaxies, which is still an open question for Astrophysics (Mediavilla et al. 2017).

Finally, once all this theoretical study is completed, and if positive results are found, we will proceed to apply for observation time in the state-of-the-art telescopes with Integral Field Units instruments in order to observe the most promising lens systems candidates.

6 Conclusions

Firstly, a general behaviour for lens systems with shear is inferred from section 4.2: the images obtained are deformed along the elongated axis whereas they are compressed in the perpendicular direction (Figure 4). Another outcome from this section is that different centroid displacements can be obtained with the same lens system and source depending on where the source is placed.

According to the comparisons made in section 4.3 (Figures 5 and 6) the code employed in this work can reproduce the results of Treyer & Wambsganss (2004). In their work the deviations of the centroid with respect to an initial position as the source moves with respect to the lens galaxy were studied. Even if the layout is not exactly the same for both simulations, the general behaviour is preserved (Figure 5 and Figure 6 (a)). The main drawback of their approach is the accumulation of displacement in the direction of movement because it masks the displacement due to microlensing. Moreover, in order to obtain measurable displacements produced by the microlensing effect, the lens system must be tracked during a long period of time, order of months or years according to Treyer & Wambsganss (2004).

Given the limitations of the previous approach, a new method has been tested in this work. This technique will provide, in a single epoch of measurements, the centroid displacement of a relatively small region of the source with respect to a larger region, insensitive to microlensing. In order to prove the validity of this method, three lens systems with different parameters have been simulated.

In the first place, it has been studied the dependence of the centroid shift with respect to the size of the source. The expectation was that the displacement of the centroid will decrease as the source becomes larger. We confirm this hypothesis when the fraction of mass in stars is relatively small (Figure 8 (b) and (c)). However, this is not the tendency shown by the system with a large fraction of mass in stars (Figure 8 (a)). For this reason, a requirement for applying this method is to consider only lens systems with a relatively low fraction of mass in compact objects.

Even if the lens systems follow the expected tendency, the centroid displacements should be large enough to be measurable. To analyze this question, a study on the correlation between the centroid shift and the magnification has been carried out. The initial assumption is that, the greater the magnification, the larger the shifts. Nonetheless, only systems with low macro-magnification will hold this positive correlation (Figure 10 (b)). Systems with high macro-magnification (in absolute value) deform the space greatly. This deformation breaks the correlation between the caustic position (where the magnifications are very high) and the region where the stars can have an important effect in the deflection of light of the source. Since this correlation is not maintained, then regions with high magnification do not have to correspond to regions where the deformation of the source is greater.

On contrast, lens systems with large Einstein's angle and large macro-magnification will have on average larger displacements of the centroid. The reasons behind are that the distortions of the stars are amplified by the macro-magnification and that the physical scale is proportional to the Einstein's angle. So, despite the fact that these systems will not follow the aforementioned correlation, it is probable that the displacements they produce will be larger enough to be measured.

Another parameter to take into account is the mean separation between stars. This distance gives a characteristic source size for the system. In order to obtain the largest centroid shift for the object source, its size must be much smaller than this characteristic source. Additionally, to reduce the error induced by the shift of the reference object, the source for reference must be larger than the characteristic source.

In conclusion, not all the lens systems are suitable to measure the centroid shift of an object with the proposed single epoch procedure. The main conditions that they must satisfy are: low mass in stars, large Einstein's angle, large macro-magnification (in absolute value), object under study smaller than the characteristic size and reference object larger than the characteristic size. Even though a system produces displacements below the current resolution limit, if its macro-magnification is low enough, then events with higher magnification can be selected in order to obtain greater shifts.

Bibliography

Chang, K. & Refsdal, S. 1984. "Star disturbances in gravitational lens galaxies". Astronomy and Astrophysics, 132, 168.

Jiménez-Vicente, J., Mediavilla, E., Kochanek, C.S., Muñoz, J.A., Motta, V., Falco, E. & Mosquera, A.M. 2014. "The Average Size and Temperature Profile of Quasar Accretion Disks". The Astrophysical Journal, 783(1), 47.

Kayser, R., Refsdal, S. & Stabell, R. 1986. "Astrophysical applications of gravitational micro-lensing". Astronomy and Astrophysics, 166, 36.

Kochanek, C.S., Falco, E.E., Impey, C., Lehar, J., McLeod, B. & Rix, H.W. Last updated 2015. "CASTLES Survey". https://www.cfa.harvard.edu/castles/, viewed 8 Janary 2020.

Lindegren, L. 1978. "Photoelectric Astronomy. A comparison of methods for precise image location". IAU Colloquium 48, Vienna, Austria, 197.

Mosquera, A.M. & Kochanek, C.S. 2011. "The Microlensing Properties of a Sample of 87 Lensed Quasars". The Astrophysical Journal, 738(1), 96.

Mediavilla, E., Muñoz, J.A., Falco, E., Motta, V., Guerras, E., Canovas, H., Jean, C., Oscoz, A. & Mosquera, A.M. 2009. "Microlensing-based Estimate of the Mass Fraction in Compact Objects in Lens Galaxies". The Astrophysical Journal, 706(2), 1451.

Mediavilla, E., Muñoz, J.A., Garzón, F. & Mahoney, T.J. 2016. "Astrophysical Applications of Gravitational Lensing. XXIV Canary Islands Winter School of Astrophysics". First Edition, Cambridge University Press.

Mediavilla, E., Jiménez-Vicente, J., Muñoz, J.A., Vives-Arias, H. & Calderón-Infante, J. 2017. " Limits on the Mass and Abundance of Primordial Black Holes from Quasar Gravitational Microlensing". The Astrophysical Journal Letters, 836(2), L18.

Muñoz, J.A., Mediavilla, E., Kochanek, C.S., Falco, E.E. & Mosquera, A.M. 2011. "A Study of Gravitational Lens Chromaticity with the Hubble Space Telescope". The Astrophysical Journal, 742(2), 67.

Oguri, M., Schrabback, T., Jullo, E., Ota, N., Kochanek, C.S., Dai, X., Ofek, E.O., Richards, G.T., Blandford, R.D., Falco, E.E. & Fohlmeister, J. 2013. "The Hidden Fortress: structure and substructure of the complex strong lensing cluster SDSS J1029+2623". Monthly Notices of the Royal Astronomical Society, 429, 482.

Shakura, N.I. & Sunyaev, R.A. 1973. "Black Holes in Binary Systems. Observational Appearance". Astronomy and Astrophysics, 24, 337.

Schneider, P. & Weiss, A. 1987. "A gravitational lens origin for AGN-variability? Consequences of micro-lensing". Astronomy and Astrophysics, 171, 49.

Schneider, P. & Weiss, A. 1988. "Light Propagation in Inhomogeneous Universes". The Astrophysical Journal, 327(1), 526.

Schneider, P., Ehlers, J. & Falco, E.E. 1992. "Gravitational Lenses". First Edition, Springer.

Schneider, P. 2006. "Extragalactic Astronomy and Cosmology". Second Edition, Springer, Section 2.5.

Treyer, M. & Wambsganss, J. 2004. "Astrometric microlensing of quasars. Dependence on surface mass density and external shear". Astronomy and Astrophysics, 416, 19.

Wambsganss, J. 1998. "Gravitational Lensing in Astronomy". Living Reviews in Relativity, 1, 12.

Wambsganss, J. 2006. Part 4 in: Kochanek, C.S., Schneider, P. & Wambsganss, J. "Gravitational Lensing: Strong, Weak & Micro". Springer-Verlag, 457.

Wright, E.L. 2006. "A Cosmology Calculator for the World Wide Web". Publication of the Astronomical Society of the Pacific, 118, 1711. www.astro.ucla.edu/∼wright/CosmoCalc.html, viewed 8 January 2020.

Zu, Y., Kochanek, C.S. & Peterson, B.M. 2011. "An Alternative Approach to Measuring Reverberation Lags in Active Galactic Nuclei". The Astrophysical Journal, 735(2), 80.

Appendix: Consistency of the results

A.1 Stars effect

The criterion expressed in equation (27) gives the size of the image plane. However, since the stars' distribution is finite, there will be an overall pull for the deflection of light that will disturb the real centroid (which is the one given by an infinite random distribution of stars). A way to study this tidal pull is to place a source in a lens system and compute its centroid shifts for different sizes of the image plane and, therefore, different total number of stars. To avoid the variance induced by different positions of stars, when a larger map of stars' distribution is computed, the stars' positions of the smaller maps are maintained and we only add stars in the increased outer region.

The calculations in this case are performed for the lens system C and for a source of radius 7 ld with constant emission profile. The different centroid shifts are shown in Figure 11 for five sizes of the image plane. The reference for all these shifts is the centroid if all the mass were smoothly distributed, which remains the same independently of the size of the image plane. As it can be seen, the centroid varies up to 14 μas depending on how many stars are placed. The mean shift is 19.03 μas and the standard deviation of the mean is 2.95 μas, this gives a relative error for the centroid determination of 15.5%.

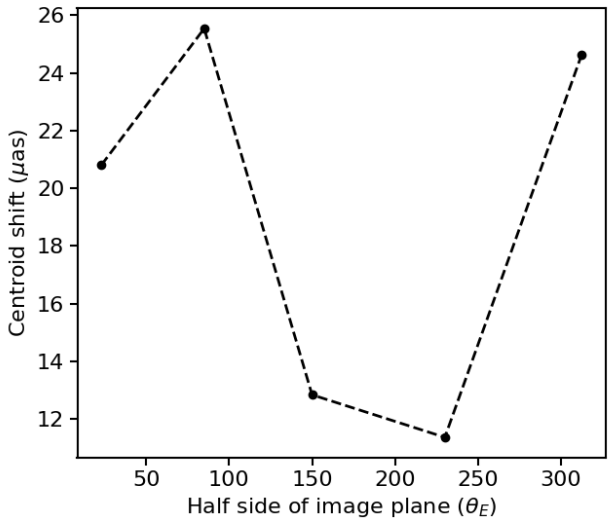

Figure 11: Dispersion of the centroid shift in microarcseconds depending on how large the image plane is, i.e., how many stars are considered. The computations have been carried out for lens system C with a source of radius 7 ld.

This error in the centroid determination could be eliminated by considering an extreme large image plane with consequently a huge number of stars. However, this procedure is not possible due to computational limits, for memory space as well as for the required time. In spite of that, this effect can be minimized by averaging different

stars' distributions which will have different total tidal pull. This is the case for Figure 8, where 20 different distributions have been considered. On the other hand, Figure 10 was obtained only for one distribution of stars so the results can be affected by this phenomenon indeed. Nevertheless, this tidal effect only alters the value of the scale of the displacements whereas the general dependence with the magnification is not affected. In addition, this relative error is obtained for system C which is the system with fewer surface mass density in stars. Therefore, its tidal effects will be stronger since the relative impact of fluctuations is expected to decrease with $1/\sqrt{n_s}$. Consequently, this error must be taken as an upper limit of the systematic errors induced by the overall tidal pull of the stars. And it will only be relevant to the values of the displacements where just one stars' distribution has been considered.

A.2 Resolution effect

Another cause of uncertainties in the centroid determination can be the finite resolution considered. In all the computations, the resolution in the image plane and in the source plane is the same in angular scale. The minimum resolution in the source plane is given by the criterion that the radius of the smallest source will be sampled with at least 5 pixels. However, this resolution cannot be enough to distinguish small deviations in the centroid. This is the case for the simulation of system B in Figure 8. The displacements that produces are intrinsically small so it is necessary to enlarge the resolution by a factor of 5 in order to appreciate their variations. This increase of the resolution provokes that the radius of the smallest source has been sampled with 26 pixels.

It can be argued that an increase in the resolution will produce a better centroid determination since the errors associated to the pixel size are reduced. In addition, when a ray of the source falls in a image pixel, it is possible that the area associated to this pixel will be larger than the actual area of that image. This effect is corrected partially by increasing the resolution. However, since this is computationally expensive, another approach is to eliminate isolated pixels which are the most prone to produce this error. If there is a group of pixels together, the actual image in this region will have a considerable spatial extent, then it is not likely that the size given by the pixels will be highly overestimated.

In Table 2, the centroid shifts obtained for a resolution of 1 pix = 0.026 θ_E and for the double of resolution (1 pix = 0.013 θ_E) are shown. Additionally, the centroid displacements have been calculated excluding the isolated pixels for both resolutions. These computations have been done for lens system A with sources radius of 5, 56 and 200 ld; which are the smallest, the characteristic and the largest source considered in Figure 8 (a), respectively.

As it can be seen for all the sources, the centroid determination do not vary considerably between simple resolution and double resolution. On the other hand, larger differences are observed between the calculations without isolated pixels and with all the pixels. The difference is caused because this procedure also eliminates pixels that may have the correct, or even more, spatial extent. Due to this reason, this technique has not been applied in the derivation of the results.

Another feature that shows this table is that the relative errors decrease as the source grows larger. The reason is that the source is sampled with more pixels and, in consequence, there will be more rays from the source in the image plane to compute its centroid. To sum up, given that the centroid do not vary excessively when there is more resolution, it has been concluded that the results for the centroid shifts are sufficiently precise if a source is sampled with at least 5 pixels for its radius and if the same angular extent for the pixels in the image and in the source plane is chosen.

Source radius (ld)	Centroid shift (μas)				Relative error (%)
	Simple resolution	Simple resolution without isolated pixels	Double resolution	Double resolution without isolated pixels	
5	9.49	11.34	9.26	9.83	4.69
56	7.69	7.60	7.69	7.73	0.36
200	12.53	12.63	12.58	12.59	0.16

Table 2: Centroid displacements determinations in μas for system A with different source sizes (in light-days). The centroid of the images have been computed for a resolution of 1 pix = 0.026 θ_E (simple resolution) and for a resolution of 1 pix = 0.013 θ_E (double resolution). For both resolutions, the centroid has been computed with all the pixels and removing the isolated pixels. The relative error has been computed as the mean standard deviation divided by the mean.